Journal of Alloys and Compounds 509 (2011) 8707–8715

Contents lists available at ScienceDirect

Journal of Alloys and Compounds

journal homepage: www.elsevier.com/locate/jallcom

Self-aligned TiO_2 nanotube arrays produced by air-cathode as electrode

Jeremy C.H. Koh, Zainal Arifin Ahmad, Ahmad Azmin Mohamad *

School of Materials and Mineral Resources Engineering, Universiti Sains Malaysia, 14300 Nibong Tebal, Penang, Malaysia

ARTICLE INFO

Article history:
Received 7 March 2011
Received in revised form 7 June 2011
Accepted 7 June 2011
Available online 17 June 2011

Keywords:
Titanium oxide
Nanotube
Air-cathode
Metal–air
Battery

ABSTRACT

Air-cathodes were used to produce TiO_2 nanotube arrays. The effects of pH, voltage and degradation of air-cathode in tailoring the morphologies of TiO_2 nanotube arrays were investigated. Preliminary results show that TiO_2 nanotubes could be formed and are comparable to those produced by platinum electrodes under similar conditions. The lengths and diameters of TiO_2 nanotube arrays obtained are in the range of 1.0–2.2 μm and 40–150 nm, respectively. It is found that the rate of formation of the nanotubes is closely related to the pH of the solution. Air-cathodes are found to have relative low values of mass loss rates.

1. Introduction

Nanostructured titanium dioxide (TiO_2) materials have been investigated extensively in recent years for application in photovoltaic electrodes, coating and corrosion protections. Various approaches have been studied and developed to produce nanostructured TiO_2, the most notable of which include the sol–gel technique [1,2], template-assistant deposition [3], seeded growth [4], hydrothermal processes [5], and metal anodization [6]. Among these techniques, the metal anodization process has been widely regarded as a straight forward surface treatment technique that can be easily automated to produce highly ordered self-aligned TiO_2 nanotube arrays with decent qualities. There are scattered reports investigating the effects of electrolyte composition, pH, voltage, time, and temperature for tailoring nanotube properties [7,8]. However, there is very little study on the effect of cathode materials used in the anodization process.

The selection of electrode influences the rates of certain reaction steps, thus influencing the overall performance [9]. For example, hydrogen evolution reaction rates vary between metals [10]. Besides, overvoltage, which is the difference in electric potential of an electrode with no current flowing through it at equilibrium and with a current flowing, affects cathodic and anodic reactions [11]. All of these parameters are closely related to the electrode material selectivity to the final products. Hence, it is understood that the selection of electrode system has to be considered carefully to produce the desired TiO_2 or other oxide nanotubes. Allam and Grimes [9] reported that TiO_2 nanotubes could be formed from different types of cathode materials, and the selection of cathode materials will affect the TiO_2 structure in one way or another. For example, the tube length, tube diameter, etc. could vary.

Apart from the properties of TiO_2 nanotube arrays, the stability of the cathode materials also has different responses to the synthetic process as well. For example, tungsten as a cathode material yields TiO_2 nanotubes with decent tube properties, but the stability of tungsten is relatively low and can be worn out quickly. Hence, it is essential to carefully select the cathode material without seriously compromising both the TiO_2 nanotube properties and the cathode material stability. A greater understanding of these relations would provide flexibility towards the process in terms of cost, time, manpower, etc.

Air-cathode generally consists of nickel foam sandwiched between a catalyst–nickel–polytetrafluroethylene (PTFE) films [12–14]. The nickel acts as a current collector that can withhold high current densities, while the catalyst mixture normally consists of MnO_2 and carbon, which acts as a catalyst for oxygen reduction and channels it into the system. A PTFE film is placed over the structure to repel atmospheric water but allow oxygen diffusion. The large surface area of the air-cathode helps it gain a large amount of reaction compared to platinum (Pt) electrodes, which have limited gas–liquid–solid three-phase boundary areas even though meshes are used [15]. Considering its high conductivity at 83.3 S cm^{-1} and high recyclability [16] the use of air-cathode could have positive impacts on the production of TiO_2 nanotube arrays. Higher conductivity would literally mean that lower voltage is required to do the same work and potentially less heat build-up that could eventually reduce the overall lower operating cost would occur. Aside from these, air-cathodes possess design flexibility that Pt electrodes do

* Corresponding author. Tel.: +60 4599 6118; fax: +60 4594 1011.
E-mail addresses: azmin@eng.usm.my, azmin@hotmail.com (A.A. Mohamad).

0925-8388/$ – see front matter © 2011 Elsevier B.V. All rights reserved.
doi:10.1016/j.jallcom.2011.06.027

not. For example, platinum cathode cannot tailor dimensions that could provide large surface areas for anodization.

In this work, the use of air-cathode to synthesize TiO_2 nanotube arrays is explored, and the effects of some anodization parameters on the stability of the air-cathode are considered. The aim is to determine whether or not air-cathode could produce TiO_2 nanotube arrays with properties similar to those obtained using Pt electrode and sustain the relevant morphologies under the same anodization conditions.

2. Experimental

2.1. Construction of casing

The plastic casing used for the anodization process was specially constructed as shown in Fig. 1. The air-cathode used, with an active area of 13.5 cm^2, was obtained from MEET, Korea. It cost 0.05 USD cm^{-2} compared to Pt electrode, which cost 44.01 USD cm^{-2}. It is composed of nickel foam coated with PTFE and a mixture of MnO_2, carbon, and PTFE binder.

2.2. Anodization process

Titanium (Ti) foils (1 cm × 2.5 cm in size, 0.127 mm thick, 99.6% purity) were purchased from STREM Chemicals. Prior anodization, the foils were degreased by sonicating in acetone and methanol for 15 min each, followed by rinsing with deionized water. The pre-cleaned foils were then dried in ambient air. Anodization was performed in a standard two-electrode bath, with Ti as the working electrode while either the air-cathode or Pt was used as the counter electrode. Pt was used as control sample. The working and counter electrodes were separated by a constant distance of 1 cm throughout the experiment. The electrolyte bath consisted of glycerol with 0.5 wt% NH_4F. The experiment was then divided into two parts, where the effects of pH and anodization voltage were investigated separately.

In the first part of the experiment, the effect of pH was investigated. The pH of the solution was adjusted to 4.0 (acidic) and 10.0 (alkaline) with the addition of sulfuric acid (H_2SO_4) or sodium hydroxide (NaOH), respectively. The bulk electrolyte bath without extra additives had a pH of 6.2. The experiment was carried out for 1 h under an anodization voltage of 20 V, which is the typical voltage [17] used to produce TiO_2 nanotube arrays. In the second part of the experiment, the effects of voltage on the TiO_2 surface morphologies produced from the electrolyte were investigated for all the pH. Anodization was carried out at room temperature (27 °C), consisting of a potential ramp (250 mV s^{-1}) from an open circuit potential to selected potentials ranging from 20 to 70 V swept across the cell by a power supply for 1 h. The as-anodized TiO_2 nanotube arrays samples were then rinsed in deionized water and ethanol before drying in ambient air.

The morphologies of the as-anodized TiO_2 nanotube arrays were characterized using field emission scanning electron microscopy (FESEM, Zeiss SUPRA 35VP). Coupled with the results of transmission electron microscopy (TEM, Philips 420T), the presence of TiO_2 nanotube arrays could be justified. The FESEM model is capable of energy dispersive X-ray (EDX) spectra determination and hence, the in situ chemical composition of the samples could be identified. The crystallographic structure and chemical composition of the TiO_2 nanotube arrays were studied by X-ray diffraction (XRD, Bruker D8 powder diffractometer).

2.3. Characterization of air-cathode

In order to investigate the air-cathode durability, another set of experiments was prepared. Ti anodization was carried out six consecutive times without changing the air-cathode. The air-cathode was weighed in order to study the stability of the air-cathode. From there, the air-cathode mass loss rate (R) in mg cm^{-2} h^{-1} could be calculated according to Eq. (1).

$$R = \frac{W_1 - W_2}{A \times t} \quad (1)$$

where W_1 and W_2 are the weights of the cathode material before and after the anodization process, respectively, A is the surface area (cm^2) of the cathode material, and t is the anodization time (h).

3. Results and discussion

3.1. Possible application air-cathode as a cathode electrode

FESEM micrographs of the as-anodized sample produced in glycerol + 0.5 wt% NH_4F at 20 V (potential ramp of 250 mV s^{-1}) for 1 h using air-cathode and Pt as cathode material are shown in Fig. 2. Fig. 2a shows that TiO_2 structures produced using the air-cathode are comparable to those produced using Pt as the cathode material (Fig. 2b). Initial results also show that there is a slight improvement in the TiO_2 surface produced using the air-cathode. Residues of oxide debris left on the surface of the products, as in Fig. 2b, could be clearly observed when Pt cathode are used, while there is only little or no oxide debris observed when air-cathodes are used. The debris formed is possibly caused by incomplete oxidation as a consequence of an insufficient length of time for anodization. However, under the same condition, the surface produced using the air-cathode was improved, prompting the idea that air-cathode are better oxidative agents.

In order to see the nanotube structure in detail, the TiO_2 nanotube arrays produced by air-cathode are magnified in Fig. 3. The FESEM image in Fig. 3a reveals the bottom of the TiO_2 nanotube arrays produced. The bottom of the nanotube arrays is closed, and the TEM image from Fig. 3b shows a tubular structure. Thus, the formation of tubular structure with open tops (Fig. 2a) and closed bottoms (Fig. 3a) is confirmed.

The proposed formation of TiO_2 uniform layer to TiO_2 nanotube arrays by this work can be summarized by Eqs. (2)–(10). As anodization initiated, at anode an initial oxide layer formed uniformly across the substrate surface due to the interactions [18]:

$$2Ti \rightarrow 2Ti^{4+} + 8e^- \quad (2)$$

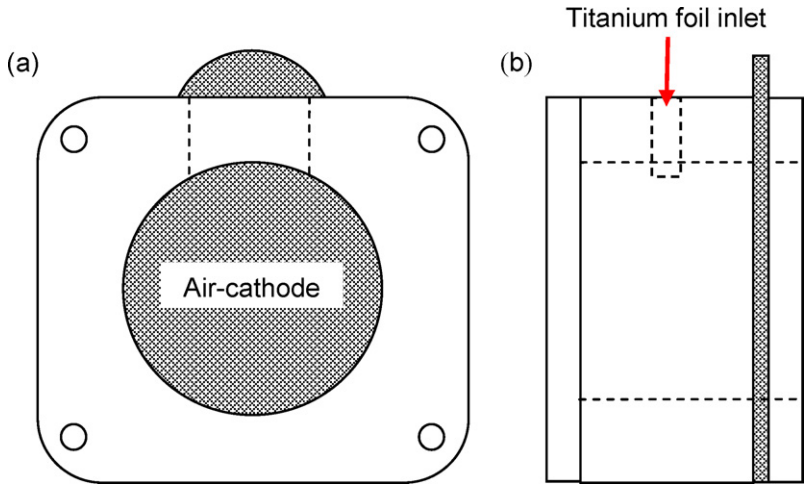

Fig. 1. Schematic diagram of the constructed case for titanium anodization: (a) front view and (b) side view.

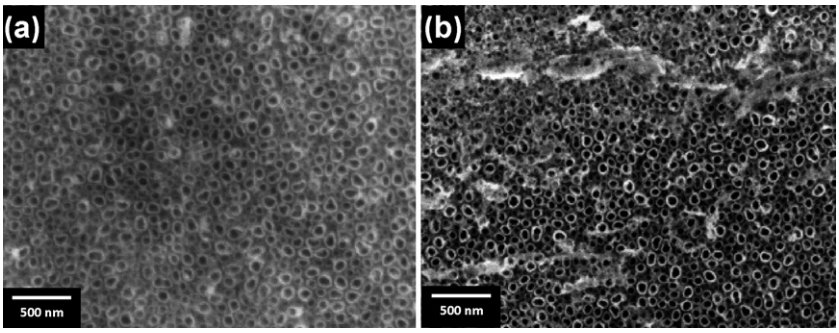

Fig. 2. FESEM micrographs of the as-anodized sample produced in glycerol + 0.5 wt% NH_4F (pH 6.2) at 20 V for 1 h using: (a) the air-cathode and (b) platinum as the cathode.

Ti^{4+} ions combine with OH^- and O^{2-} species from water.

$$6H_2O \rightarrow 4OH^- + 2O^{2-} + 8H^+ \quad (3)$$

$$Ti^{4+} + 4OH^- \rightarrow Ti(OH)_4 \quad (4)$$

$$Ti^{4+} + 2O^{2-} \rightarrow TiO_2 \quad (5)$$

$$Ti(OH)_4 \rightarrow TiO_2 + 2H_2O \quad (6)$$

In the air-cathode system, oxygen evolution normally occurs during charging for battery system (referred as anodization in this study) [12]:

$$4OH^- \rightarrow 4e^- + 2H_2O + O_2 \quad (7)$$

However this oxidation is not feasible as compared to hydrogen evolution:

$$8H^+ + 8e^- \rightarrow 4H_2 \quad (8)$$

Thus, the overall process of oxide formation is given as follows:

$$Ti + 2H_2O \rightarrow TiO_2 + 2H_2 \quad (9)$$

Subsequently, with the presence of F^- ion, the preformed oxide layer is dissolved through the formation of soluble fluoride complexes $[TiF_6]^{2-}$ as shown in Eq. (10). With prolonged anodization period, the tube forming mechanisms become governed by TiO_2 oxide formation and dissolution process [19]:

$$TiO_2 + 6F^- + 4H^+ \rightarrow [TiF_6]^{2-} + 2H_2O \quad (10)$$

3.2. Effect of pH on as anodized TiO_2 by air-cathode

Fig. 4 shows the current density transient recorded during anodization in glycerol + 0.5 wt% NH_4F at 20 V at different pH. The time dependent polarization curve, specifically the part during the first few minutes of anodization, can be ascribed to different stages of the tube growth process. Initially, there is a sudden drop (Stage I), followed by a slow and steady decrease (Stage II). Finally, a constant current density (Stage III) is observed for all the polarization curves regardless of pH level. At pH 4.0, the current density dropped drastically to around 1.2 mA cm^{-2} within a 1 min after the voltage was applied. The current density plateaus recorded at pH 6.2 and 10.0 are 0.8 and 0.5 mA cm^{-2}, respectively. The drop in current density at higher pH is due to the formation of a denser oxide layer that poses higher restriction to current penetration.

At high pH (low concentration of H^+), the hydrolysis ability of electrolytes is increased. Hence, the oxygen content is increased at high pH electrolyte and forms a denser oxide layer. Solutions at higher pH level also require longer times to reach Stage III, confirming the low oxidizability. The sudden decay of current density at Stage I could be attributed to the formation of a compact TiO_2 layer (Eq. (6)).

At this stage, the Ti foil area revealed to the electrolyte oxidizes and forms a fine layer of TiO_2 film on the electrolyte/metal interface [19]. The presence of TiO_2 at this stage is confirmed by EDX (Fig. 5). The approximate Ti:O atom ratio was determined to be 1:2, suggesting the formation of TiO_2 layer. This oxide layer will act as a natural inhibitor and elevates the resistance (due to the low conductivity of metal oxide), thus limiting the current flow, which is proportional to the thickness of this barrier layer. From here, the localized current could form pits or slits on the oxide film layer to nucleate the tube formation process. These pits will enlarge and act as sites where the oxide in these areas could be dissolved by fluoride (F^-) ions according to Eq. (10).

Here, the TiO_2 layer is attacked by F^- ions, forming the highly soluble $[TiF_6]^{2-}$ complex, and then dissolved to form porous structure (Stage II). At this stage, the dissolution of the TiO_2 layer will allow more current flow. These two processes compete between pore formation and dissolution of the oxide. Hence, at Stage III where the current density is steady, pore formation is in equilibrium with pore dissolution.

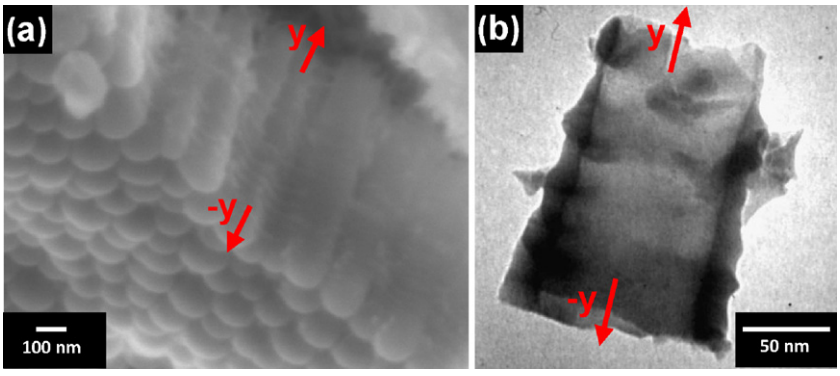

Fig. 3. (a) FESEM bottom view and (b) TEM of tubes formed using the air-cathode in glycerol + 0.5 (pH 6.2) wt% NH_4F at 20 V for 1 h. y and $-y$ refer to upward and downward directions, respectively.

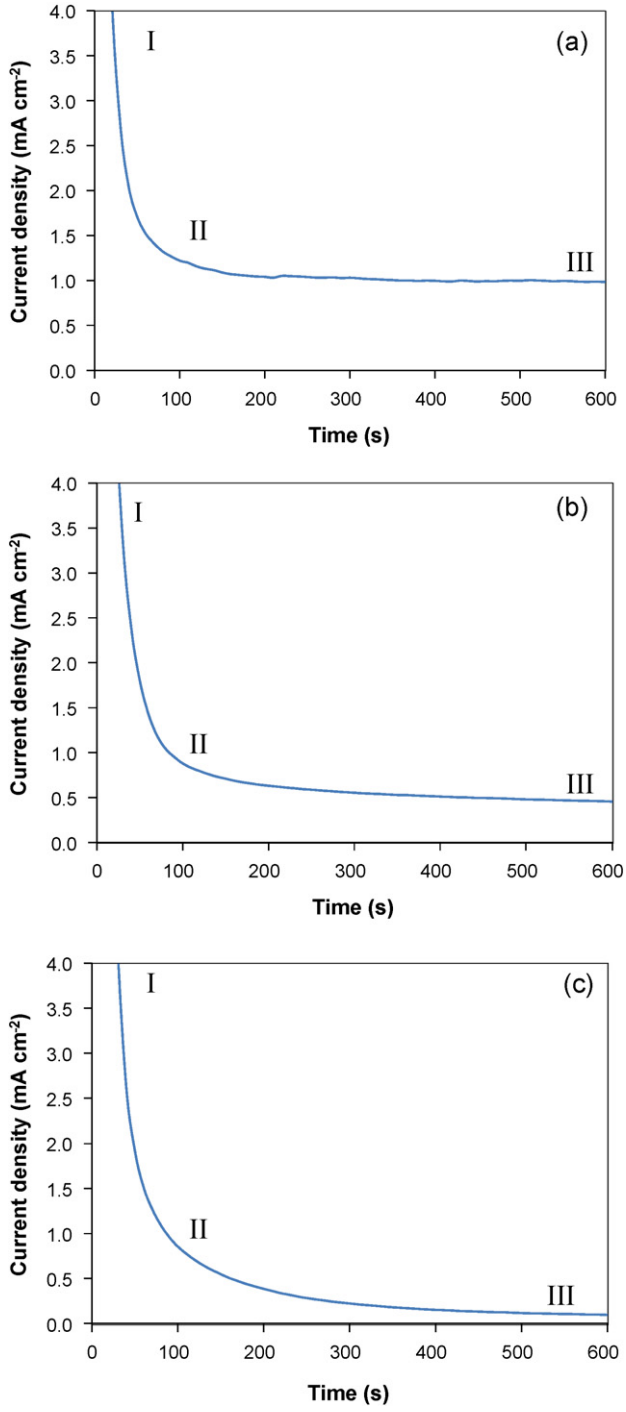

Fig. 4. Current density–time curves for titanium anodization performed at 20 V in electrolyte at (a) pH 4.0, (b) pH 6.2, and (c) pH 10.0.

The TiO_2 layer dissolution process in Stage III is closely controlled by the presence of H^+ ions, as shown in Eq. (10). As mentioned earlier, different pH levels (where the concentration of H^+ varies), could affect the dissolution process. As a result, the length of the TiO_2 tube also varies according to pH, as shown in Table 1. The average tube length produced in the electrolyte at pH 4.0 (high H^+ concentration) recorded the highest value, which is 1149 nm. The average tube length anodized under the same conditions at pH 6.2 and pH 10.0 are 1096 and 896 nm, respectively.

In order to better understand the effects of pH on tube length using the air-cathode as the electrode, the tube growth rate, where the final tube length was divided by time, was determined. The tube growth rate at pH 4.0 is 19.15 nm min^{-1}, which is the highest recorded. At pH 6.2, the tube growth rate is approximately 18.27 nm min^{-1}, while at pH 10.0, it recorded 14.93 nm min^{-1}. At higher voltage, the pH of the electrolyte also influences the oxide morphologies. The nature of the alkaline electrolytes reveals the relatively lower ability of anodic oxide formation.

Therefore, the anodic forming voltage, corresponding to the dynamic equilibrium between the oxide formation rate and chemical dissolution rate, is much lower, as shown in Fig. 6. At higher voltage, i.e., 60 V, the TiO_2 formed could be varied by different electrolyte pH, although the field-assisted tube-forming ability is elevated. The morphology image in Fig. 6a shows that, at acidic solution (pH 4.0), the TiO_2 formed still consists of tubular structures. Tubes formed at pH 6.2 maintain porous structures, and TiO_2 tubes formed at pH 10.0 are non-porous (a consequence of poor oxidation/dissolution capability), as shown in Fig. 6b and c, respectively. The dimensions and structure of the TiO_2 tubes are rather important, as they play a paramount role in order to achieve higher efficiency of photoabsorption and longer electron lifetimes, as well as longer diffusion length in the TiO_2 tube [20]. As a whole, the electrochemical growth of anodic Ti oxide occurs in the following hierarchy:

$$\text{pH}\,4.0 > \text{pH}\,6.2 > \text{pH}\,10.0$$

Aside from tube dimensions, it could also be observed that pH affects the surface topography. Fig. 7 shows the surface conditions of the as-anodized TiO_2 at 20 V (lower than 60 V) for 1 h in electrolyte at pH 4.0, 6.2, and 10, respectively. The surfaces of the three as-anodized TiO_2 samples were covered by a 'vague' layer, which consists of conglomerates of partially dissolved tubes. At pH 4.0 (Fig. 7a), the surface morphologies are relatively 'clean' and the tube ring could be seen clearly. With increasing pH (Fig. 7b), the oxide debris layer covering the surface became thicker and more significant until the tube was clotted (as can be seen in Fig. 7c). At lower pH, strong chemical dissolubility within the electrolyte could dissolve the oxide and reveal the Ti substrate. At higher pH, however, weak chemical dissolubility limits the dissolution process, leaving debris covering the top surface.

Table 1
Tube diameter and length formed at different electrolyte pH and anodization voltage.

Voltage	pH 4.0		pH 6.2		pH 10.0	
	Average length (nm)	Average diameter (nm)	Average length (nm)	Average diameter (nm)	Average length (nm)	Average diameter (nm)
20	1149	46	1096	59	896	53
30	1770	100	1284	84	879	70
40	2064	126	1692	107	1025	103
50	2053	146	1592	138	–	–
60	2189	242	–	–	–	–
70	–	–	–	–	–	–

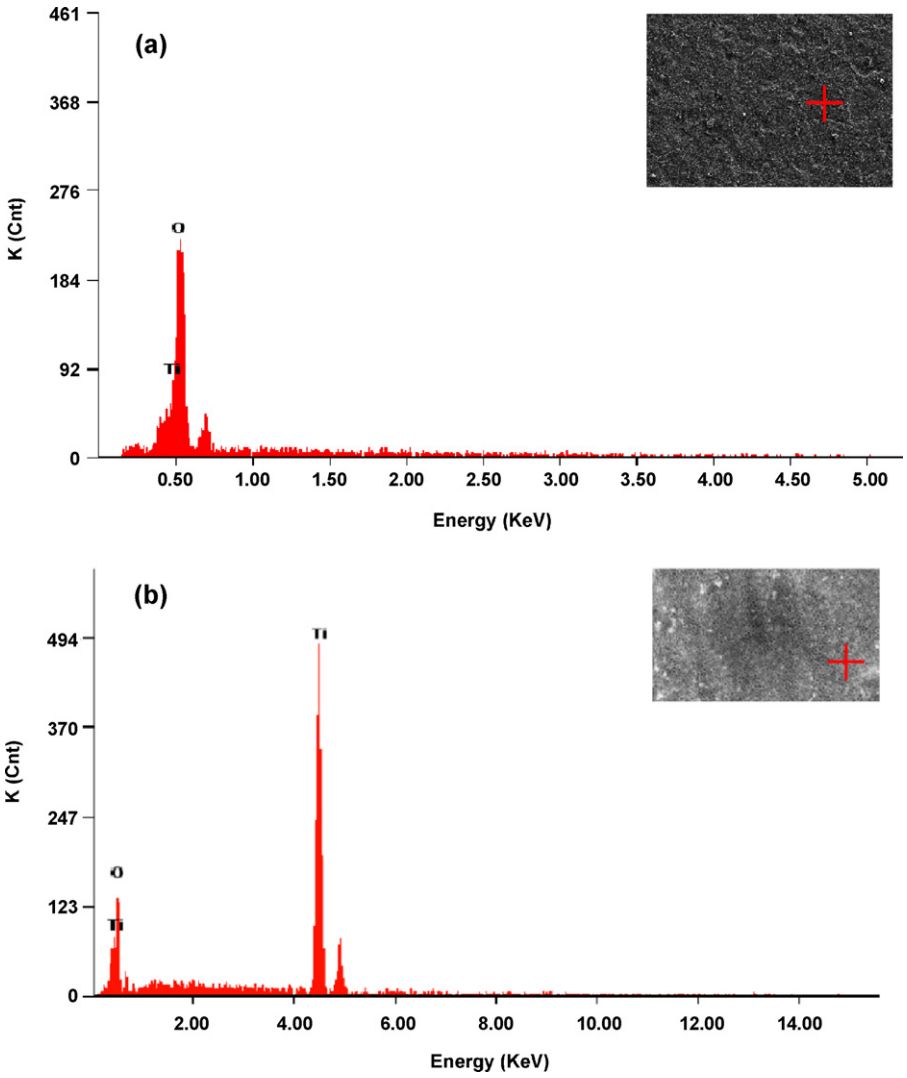

Fig. 5. EDX spectra of the Ti foil anodized in electrolyte using air-cathode as cathode with glycerol + 0.5 wt% NH_4F (pH 6.2) at 20 V after, (a) 5 min and (b) 60 min.

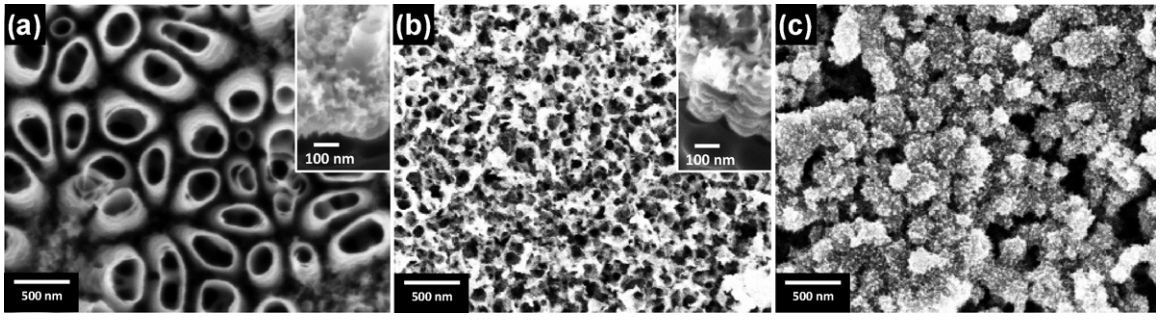

Fig. 6. FESEM of as-anodized sample at 60 V for 1 h with electrolyte at (a) pH 4.0, (b) pH 6.2, and (c) pH 10.0.

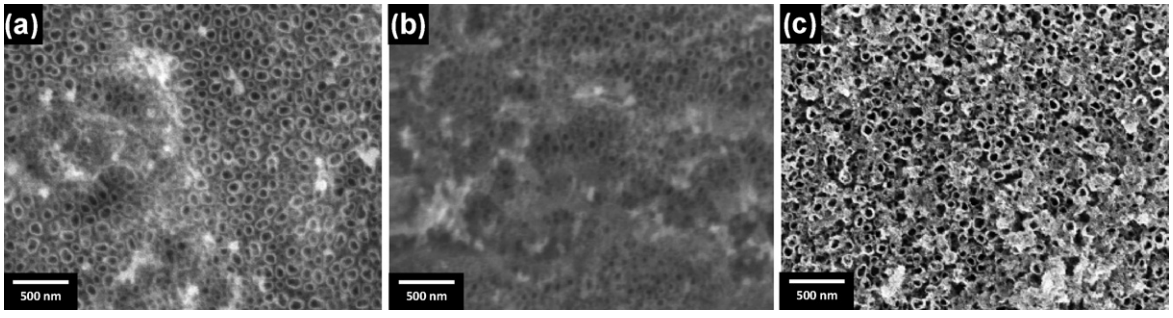

Fig. 7. FESEM of as-anodized sample at 20 V for 1 h with electrolyte at (a) pH 4.0, (b) pH 6.2, and (c) pH 10.0.

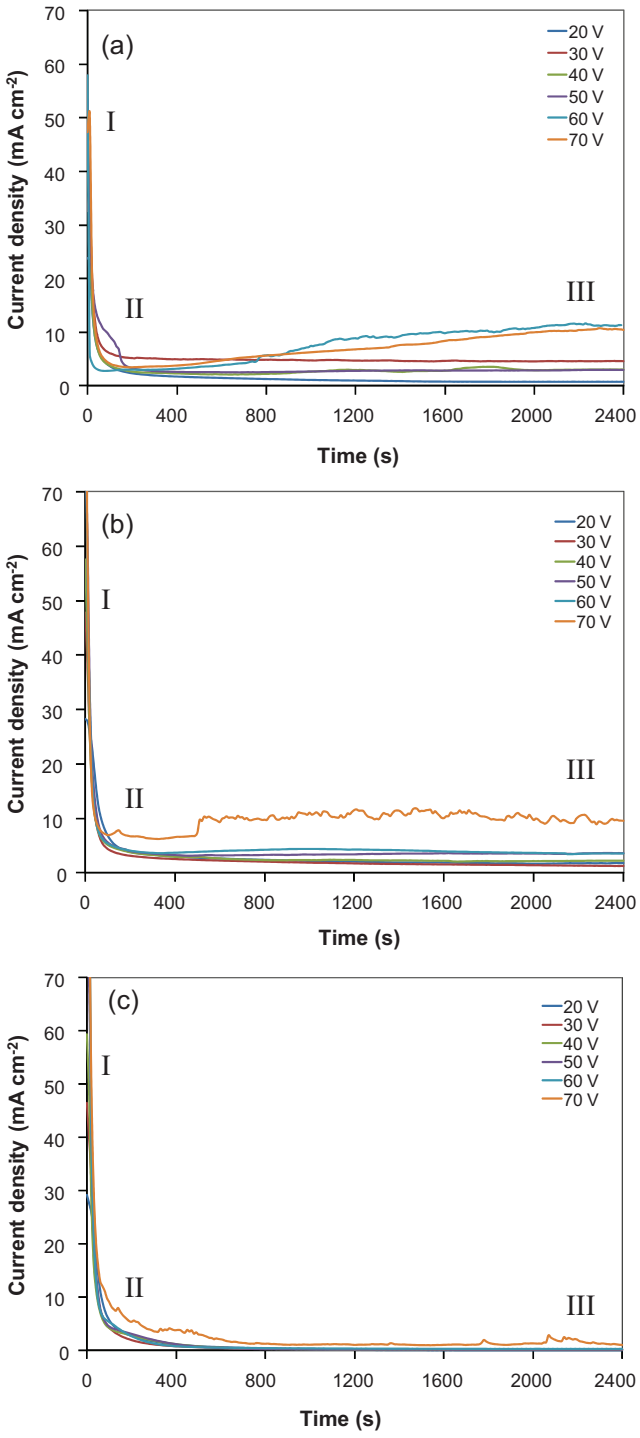

Fig. 8. Current density–time curves as a function of voltage at (a) pH 4.0, (b) pH 6.2, and (c) pH 10.0.

3.3. *Effect of voltage on as anodized TiO_2 by air-cathode*

In order to exploit the influence of the applied voltage, experiments were carried out at different anodization voltages. While the tube growth rate is closely related to pH, the tube diameter, wall thickness, and crystallinity are greatly affected by the voltage applied. For Ti anodization carried out in this experiment, a wide variety of tube diameters in the range of nano- and micron sizes could be achieved depending on the voltage applied. Fig. 8 shows that the current fluctuations at Stage III increased with increasing anodization voltage regardless of pH. At lower voltages (20–50 V), oxidation and dissolution processes occur at relatively mild or steady conditions. When the anodization voltage is increased (60 and 70 V), the diffusion of ions in the field-driven process increases and becomes unstable. The unstable oxidation and dissolution process could lead to inconsistent tube formation and hence, current fluctuations. Eventually, the tube structure will collapse when the applied voltage is too high, to the extent where the fine oxide layer constructing the tube can no longer sustain the high diffusion rate.

Fig. 9 shows FESEM images of samples anodized in glycerol + 0.5 wt% NH_4F (pH 6.2) using the air-cathode at different anodization voltages for 1 h. It could be seen that the Ti foil anodized at 20, 30, 40, and 50 V (Fig. 9a–d) all possess tube structures. However, those that are anodized at 60 and 70 V (Fig. 9e–f) have nanoporous structures (where the tube structure is destroyed by the high passivation and re-passivation rate). This is in line with the results of current density studies, where the tube structure is clearly absent in samples anodized at 70 V (Fig. 9f).

In general, when the voltage is increased, the magnitude of the localized current on the oxide surface will increase accordingly and thus create larger pits. The final diameters of the tube are highly dependent on the initial size of the pits formed. Hence, the higher the voltage applied to the system, the greater the tube diameter will be, as shown in Table 1. The increment of voltage could also remove the debris on top of the oxide surface, which is caused by weak chemical solubility as mentioned earlier. Debris could be observed on top of the surface (Fig. 9a), and this layer is removed when the voltage is increased to 30 V (Fig. 9b).

Besides the tube diameter, at relatively low voltages (20 and 30 V), the nanotube arrays appear to grow in a self-aligned formation and show high uniformity. However, when the voltage is increased beyond 30 V, the diameter exceeds 100 nm and shows a slight difference in surface morphology. It could be seen that the tubes formed consist of two distinctly different diameters, indicating that voltage plays a vital role in determining the uniformity and homogeneity of the tube formed (Fig. 9d).

Although it has been shown that the pH factor is more dominant in determining the tube length, the voltage also affects the length of the tube formed. The length of the tube formed at all pH (Table 1) increased with voltage, confirming the effect of voltage on tube length. It should also be noted that the chemical dissolution of TiO_2 occurs over the entire tube length. As a result, the tube grown for extended periods of time will become increasingly V-shaped in morphology [21,22]. In another words, the upper parts of the tubes will become significantly thinner due to longer chemical dissolution reaction times than the bottom parts of the same.

Fig. 10 shows a schematic of the chemical dissolution processes that occur during the formation of V-shaped morphology on the TiO_2 nanotube. The process starts with pit formation prior to dissolution (Fig. 10a). Dissolution occurs at all directions, forming U-shaped morphology (Fig. 10b), after which prolonged dissolution triggers tube growth, and the distance between neighboring tubes is decreased (Fig. 10c). Finally, tube possessing V-shaped morphology is formed (Fig. 10d). It can also be seen that the gaps between upper tubes (y-direction) become thinner during the V-shaped process. The thickness of the tube wall decreases from W, X, Y to Z processes.

The effects of voltage are not restricted to the dimensions of the tube formed. Fig. 11 shows the XRD pattern obtained from samples anodized in glycerol + 0.5 wt% NH_4F (pH 6.2) at different voltage for 1 h. The result shows that the anatase peak intensity generally increases with the applied voltage. Depending on the anodization conditions, the TiO_2 formed could exist in amorphous or crystalline forms (anatase, rutile, or a mixture of anatase and rutile). Initially, the raw sample mainly consists of Ti peaks with a little rutile phase. However, upon anodization at 20 V, the Ti oxide formed is in the

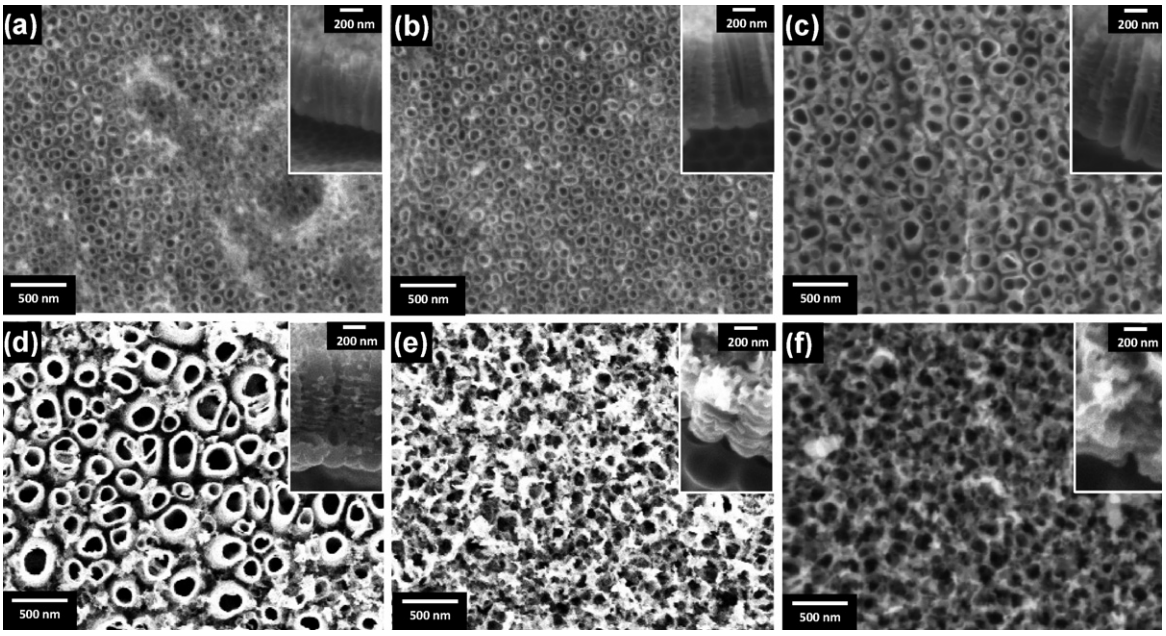

Fig. 9. FESEM micrographs of sample anodized with electrolyte of pH 6.2 for 1 h at (a) 20 V, (b) 30 V, (c) 40 V, (d) 50 V, (e) 60 V, and (f) 70 V.

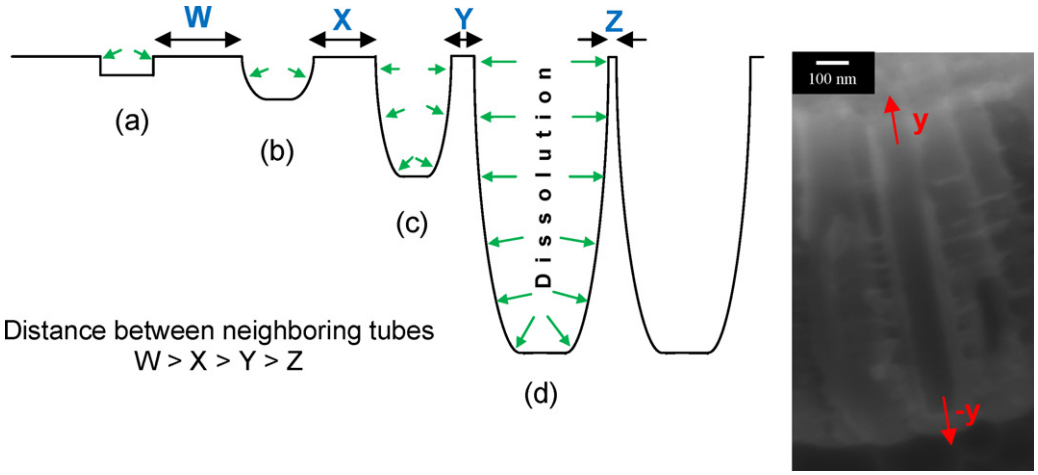

Fig. 10. Schematic diagram of the chemical dissolution process forming the V-shaped morphology on the TiO_2 nanotube. (a) Pit formed prior to dissolution, (b) dissolution occurring at all directions, forming a U-shaped morphology, (c) prolonged dissolution triggers tube growth and (d) final tube possessing V-shaped morphology. Inset: SEM image of the V-shaped tube, y and $-y$ refer to upward and downward directions, respectively.

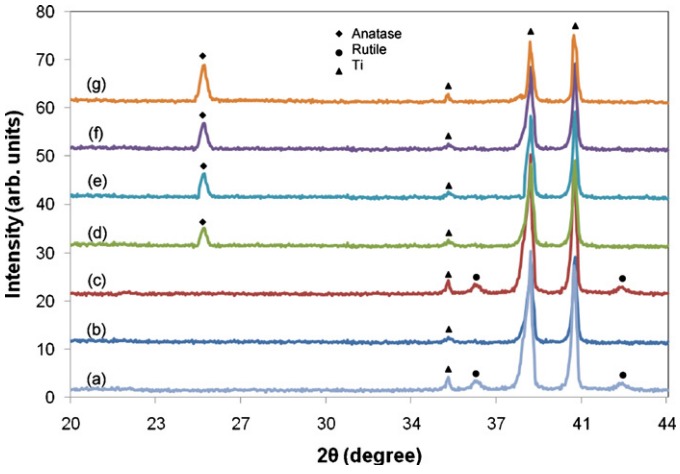

Fig. 11. XRD patterns of (a) raw sample, as well as sample anodized at pH 6.2, at voltages of (b) 20 V, (c) 30 V, (d) 40 V, (e) 50 V, (f) 60 V, and (g) 70 V.

amorphous phase. When the voltage is increased to 30 V, a minimal percentage of rutile is observed at $2\theta = 36^\circ$ and 42°. Further increments of voltage show that parts of the amorphous region are transformed to anatase crystals, where XRD analysis shows peaks at $2\theta = 25^\circ$. As a result, the peak intensity for pure Ti decreases accordingly and the intensity of anatase peaks increases with the voltage. Under these conditions, the rutile phase decreases slowly. The result also agreed with other researchers [23,24].

This transformation of amorphous to crystalline TiO_2 at elevated voltage is particularly interesting. To date, it has been widely reported that transformation of amorphous to crystalline TiO_2 would happen only when thermal treatment is applied to the as-anodized TiO_2 nanotube arrays [25]. In order to convert the amorphous tubes into crystalline anatase or rutile phase, annealing process is usually necessary. It is reasonable to assume that the crystallization process developed after the electrical breakdown, which is triggered by local exothermic heat with increasing voltage. Moreover, considering the anodization process is field driven, higher anodization voltage would favor high ion diffusivity which would lead to crystallization. Nonetheless, Jamieson and Olinger

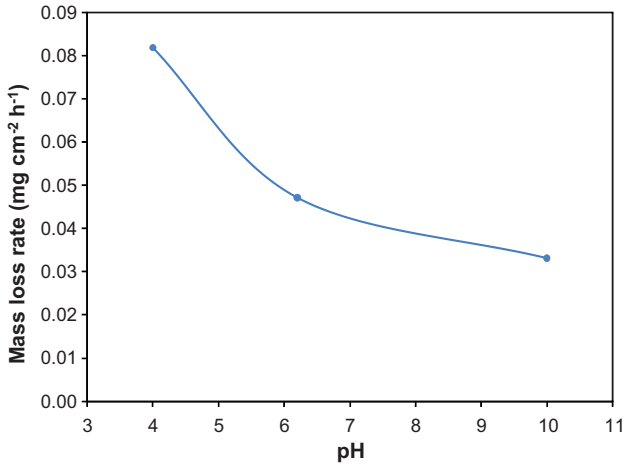

Fig. 12. Air-cathode mass loss rate as a function of pH anodized at 20 V for 1 h.

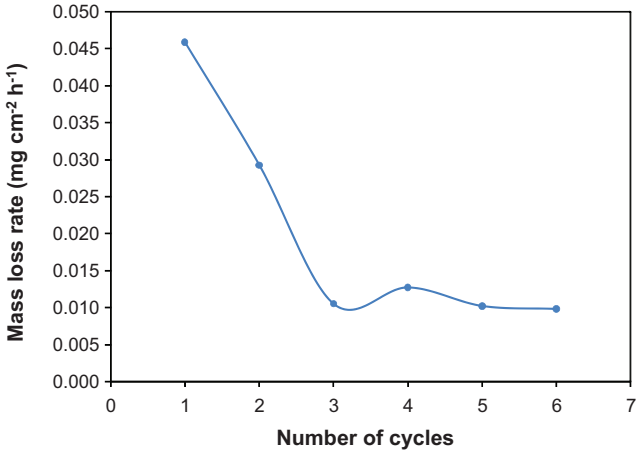

Fig. 14. Air-cathode mass loss rate as a function of number of cycles anodized at 20 V in electrolyte with pH 6.2.

[26] reported that anatase is thermodynamically always unstable. Thus the persistence or formation of anatase under this condition should be regarded as a consequence of sluggish reaction kinetics or metastable crystallization. Meaning that, the as-anodized TiO_2 nanotube arrays are weakly crystallized as been confirmed by the low anatase peak intensity.

3.4. Air-cathode stability

Figs. 12–14 shows air-cathode mass loss rates as a function of pH, voltage, and number of cycles used, respectively. This is the first time that the stability of a material during anodization is being evaluated to the extent where the effect of pH, voltage, and number of cycles are considered. Fig. 12 shows the mass loss rate as a function of pH was recorded at a cell voltage of 20 V. Electrolytes with pH 4.0 recorded the highest mass loss rate at 0.08191 mg cm^{-2} h^{-1}. Electrolytes with pH 6.2 and 10.0 recorded a decreasing trend of 0.04716 and 0.03315 mg cm^{-2} h^{-1}, respectively. At low pH (pH 4.0), the high concentration of H^+ ions results in higher passivation and re-passivation activities that could lead to high current flows in the system. As a result, the overwhelming built-up charge could damage the air-cathode. When the pH of the electrolyte is increased, mild TiO_2 tube formation processes could yield lower mass loss rate.

When the air-cathode was subjected to different voltages, the mass loss rate increased with increasing voltage; this could be because of the same reasons given for the effect of pH. That is, higher voltages could allow higher current densities to flow. Fig. 13 shows the mass loss rate as a function of voltage recorded in the electrolyte with pH 6.2 for 1 h. The mass loss rate recorded for 20 V is 0.04716 mg cm^{-2} h^{-1}. This value has increased steadily to 0.08191 mg cm^{-2} h^{-1} when anodization was performed at 70 V.

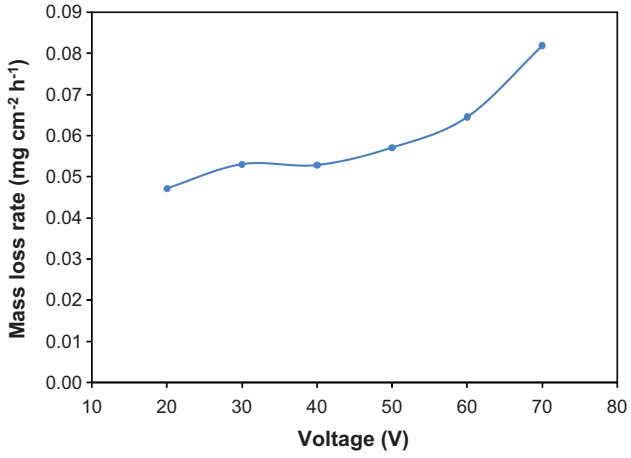

Fig. 13. Air-cathode mass loss rate as a function of voltage in electrolyte with pH 6.2 for 1 h.

While both pH and voltage induced significant impacts on air-cathode stability, the number of cycles for which the air-cathode is used appears to show slightly different behaviors. Fig. 14 shows the mass loss rate as a function of number of cycles the air-cathode is used for anodization at 20 V for 1 h. The air-cathode is used for 6 consecutive cycles without changing. A completely new set of electrolyte and Ti foil was used to eliminate unnecessary determining factors. Initially, it could be seen that the mass loss rate was high. During the first usage, the mass loss rate recorded was 0.04587 mg cm^{-2} h^{-1}; during the second usage, a drop in the loss rate to 0.02928 mg cm^{-2} h^{-1} was observed. However, beginning from the third usage onwards, the mass loss rate recorded a near constant trend. The third usage recorded a mass loss rate of 0.010533 mg cm^{-2} h^{-1}, which is more than a 60% drop from the second usage. The fourth, fifth, and sixth usages of the air-cathode recorded mass loss rates of 0.012733, 0.012033, and 0.009833 mg cm^{-2} h^{-1}, respectively. The high mass loss rate at first cycle attributed to dissolution of carbon and active material from air-cathode. Normally, at the surface of air-cathode these materials are not bound strongly by binder and easy to dissolve into electrolyte. The electrolyte changed from clear to a black color after the cycle. In previous report we also reported the changes of air-cathode upon cycling [13].

4. Conclusion

The present work investigates the possibility of fabricating self-organized TiO_2 nanotube arrays using relatively cheap but compatible air-cathodes as cathode. Results showed that the TiO_2 nanotube arrays formed using such material are of decent quality and comparable to those produced using Pt as a cathode material. Tube formation rates were found to decrease with increasing pH. The anodization voltage was dominant in controlling the diameter of the tubes formed. The crystallographic structure was found to be closely connected to the anodization voltage. XRD results also confirmed that no pollution towards the as-anodized sample occurred, thus eliminating the concern of pollution. The air-cathode showed high durability with repeated usage. Combining all these results, it appears that the less expensive and highly recyclable air-

cathode can replace Pt for fabricating decent TiO_2 nanotubes via anodization.

Acknowledgements

J.C.H.K would like to thank Universiti Sains Malaysia (USM) for their continuous support via a USM-RU-PRGS (8031035) and USM Fellowship. A.A.M would like to thank USM for their Short Term Grant (60311004).

References

[1] H. Dai, Y. Chi, X. Wu, Y. Wang, M. Wei, G. Chen, Biosensors and Bioelectronics 25 (2010) 1414–1419.
[2] D. Fang, K. Huang, S. Liu, Z. Luo, X. Qing, Q. Zhang, Journal of Alloys and Compounds 498 (2010) 37–41.
[3] Y.-F. Tu, S.-Y. Huang, J.-P. Sang, X.-W. Zou, Journal of Alloys and Compounds 482 (2009) 382–387.
[4] L. Tian, S.-i. Mho, Solid State Communications 125 (2003) 647–651.
[5] Y.-C. Liu, J.-M. Huang, C.-E. Tsai, T.C. Chuang, C.-C. Wang, Chemical Physics Letters 387 (2004) 155–159.
[6] T.-H. Fang, K.-T. Wu, Electrochemistry Communications 8 (2006) 173–178.
[7] V. Vega, M.A. Cerdeira, V.M. Prida, D. Alberts, N. Bordel, R. Pereiro, F. Mera, S. Garc, M. Herndez-Vez, M. Vquez, Journal of Non-crystalline Solids 354 (2008) 5233–5235.
[8] D.-J. Yang, H.-G. Kim, S.-J. Cho, W.-Y. Choi, Materials Letters 62 (2008) 775–779.
[9] N.K. Allam, C.A. Grimes, Solar Energy Materials and Solar Cells 92 (2008) 1468–1475.
[10] H.J. Flitt, J.O.M. Bockris, International Journal of Hydrogen Energy 6 (1981) 119–138.
[11] A.J. Nozik, Annual Review of Physical Chemistry 29 (1978) 189.
[12] A.A. Mohamad, Journal of Power Sources 159 (2006) 752–757.
[13] A.A. Mohamad, N.S. Mohamed, Y. Alias, A.K. Arof, Journal of Power Sources 115 (2003) 161–166.
[14] A.A. Mohamad, Corrosion Science 50 (2008) 3475–3479.
[15] K. Akuto, M. Takahashi, Y. Sakurai, Journal of Power Sources 103 (2001) 72–79.
[16] S.H. Kim, Y.I. Kim, J.H. Park, J.M. Ko, International Journal of Electrochemical Science 4 (2009) 1489–1496.
[17] J.M. Macak, P. Schmuki, Electrochimica Acta 52 (2006) 1258–1264.
[18] A. Jaroenworaluck, D. Regonini, C.R. Bowen, R. Stevens, D. Allsopp, Journal of Materials Science 42 (2007) 6729–6734.
[19] E. Sennik, Z. Colak, N. Kilinc, Z.Z. Ozturk, International Journal of Hydrogen Energy 35 (2010) 4420–4427.
[20] R. Beranek, J.M. Macak, M. Gatner, K. Meyer, P. Schmuki, Electrochimica Acta 54 (2009) 2640–2646.
[21] K. Yasuda, P. Schmuki, Electrochimica Acta 52 (2007) 4053–4061.
[22] F.M. Bayoumi, B.G. Ateya, Electrochemistry Communications 8 (2006) 38–44.
[23] M. Bestetti, S. Franz, M. Cuzzolin, P. Arosio, P.L. Cavallotti, Thin Solid Films 515 (2007) 5253–5258.
[24] M.V. Diamanti, M.P. Pedeferri, Corrosion Science 49 (2007) 939–948.
[25] K. Prasad, D.V. Pinjari, A.B. Pandit, S.T. Mhaske, Ultrasonics Sonochemistry 17 (2010) 409–415.
[26] J.C. Jamieson, B. Olinger, The American Mineralogist 54 (1969) 1477–1481.